Desalination and Water Treatment
www.deswater.com

doi: 10.5004/dwt.2021.26725

213 (2021) 418–430
February

Removal of methylene blue from aqueous solution by functionalized UiO-66 with basic moiety

Shucui Han[a], Jinbei Yang[b,*], Xueting Lin[b]

[a]*Department of Chemical Engineering, Zhicheng College of Fuzhou University, Fuzhou 350002, Fujian, China, Tel. +86-13960885921; email: hanshucui@163.com*
[b]*Fujian Provincial Key Laboratory of Coastal Basin Environment, Fuqing Branch of Fujian Normal University, Fuzhou 350300, Fujian, China, Tel. +86-15280192415; emails: yangjinbei@sina.com (J. Yang), linxter@qq.com (X. Lin)*

Received 21 April 2020; Accepted 17 October 2020

ABSTRACT

In this study, the adsorptive removal of methylene blue from aqueous solution was carried out by Zr-containing metal-organic frameworks (MOFs). UiO-66, prototypes of MOFs, was used as an adsorbent with or without functionalization of free amino groups. Although the porosity and surface area of the functionalized UiO-66 (UiO-66-NH_2) were smaller than that of the original UiO-66, its adsorption capacity for methylene blue increases significantly with the functionalization. The improvement of the performance of UiO-66-NH_2 can be attributed to electrostatic interaction between the cationic dye and the negatively charged surface of adsorbent, which is helpful for the adsorption of methylene blue. In order to study the adsorption characteristics, the effects of various operating parameters such as adsorbent dosage, shaking speed, pH, initial concentration of methylene blue, and temperature were investigated in a batch adsorption. The adsorption isotherm and kinetic data of methylene blue onto UiO-66-NH_2 are best fitted by Redlich–Peterson and Elovich models, respectively. The adsorption process is an exothermic and of the multilayer variety. Thermodynamic parameters such as ΔG, ΔH, and ΔS were determined, which indicate that the adsorption process endothermic and spontaneous. Moreover, the UiO-66-NH_2 adsorbent can be easily regenerated and reused by ethanol as eluent and the adsorption capacity decreases by only 7.6% after five adsorption–desorption cycles. Therefore, MOFs functionalized with basic site, such as UiO-66-NH_2, can be employed as an environmentally friendly adsorbent for the methylene blue removal from wastewater.

Keywords: Methylene blue; UiO-66-NH_2; Adsorption; Kinetic; Thermodynamics

1. Introduction

In recent years, China's organic dye industry has developed rapidly. Throughout the production process of organic dye, a large amount of dye wastewater is generated, especially in the processes of sulfonation, nitration, reduction–oxidation, diazotization, and salting out. Organic dyes contain chemical ingredients that are harmful to humans and the environment, most of which have carcinogenic effects on humans and mammalian organisms [1,2]. Methylene blue, classified as cationic dye category (Fig. 1), is one of the major pollutants of organic dyes, which is widely used in the fields of papermaking, printing and dyeing, and textile industry [3]. Methylene blue is relatively stable in water, and has a strong resistance to oxidation and photolysis. Therefore, Methylene blue can be present in large quantities in wastewater and cause environmental pollution, and it is necessary to treat methylene blue-containing wastewater before discharge.

* Corresponding author.

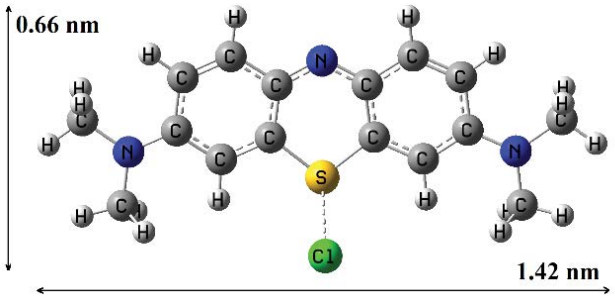

Fig. 1. Molecular structures and sizes of methylene blue.

There are many methods that have been applied in the removal of dyes from an aqueous solution including chemical oxidation [4,5], photodegradation [6,7], membrane separation [8,9], electrochemical treatment [10,11], biological techniques [12,13], and adsorption [14–16]. Among the methods used, photodegradation is considered as a promising way of degrading dye [17,18]. However, it also has disadvantages, such as the need to add an additional oxidant, a narrow UV absorption range, low light energy utilization, and only effective for low-concentration dyes. Adsorption is recognized to be one of the most competitive technologies, which has the characteristics of high efficiency, low cost, and recyclability, and is widely used for dye-containing wastewater treatment [19]. Nowadays, there are many adsorbents that have been reported for the dye's removal, such as activated carbon [20,21], industry solid waste [22,23], graphene [24], clay minerals [25,26], agricultural waste [27,28], etc. Naushad et al. [29] developed activated carbon modified by 2-amino-5-guanidinopentanoic acid for the removal of methylene blue from an aqueous solution. Regeneration results showed that the adsorbent can retain methylene blue after four cycles. Anitha et al. [30] synthesized a newly nano-sized chitosan/PVA composite which was an effective adsorbent to remove Eosin Yellow dye from the aqueous solution. The prepared material could be used for recycling purposes and also be successfully employed for industrial wastewater. Tatarchuk et al. [31] synthesized cobalt-zinc ferrite nanoparticles which could be used as magnetic adsorbents to remove cationic and anionic dyes.

Notwithstanding, there are still various challenges in the adsorption process, such as the limited selectivity and adsorption capacity for removing low-concentration adsorbates, limited operating pH range, and adsorbent regeneration. Metal-organic frameworks (MOFs) are porous coordinated functionalized materials with a unique topological crystalline network structure, which are mainly synthesized through the connection of metals or metal clusters with flexible organic ligands [32]. Compared with traditional adsorbents, MOFs can be considered as a potential and environmentally friendly material for dye adsorption and selective separation due to the multi-selectivity, high surface area, and good stability [33]. Therefore, in this work two Zr-containing MOFs, UiO-66 with and without functionalization of amino groups, were synthesized by solvothermal method and characterized by X-ray diffraction (XRD), Fourier transform infrared (FT-IR), scanning electron microscopy (SEM), and Brunauer–Emmett–Teller (BET), which were further used as adsorbent for the methylene blue removal from aqueous solution via a batch adsorption. Moreover, the effect of adsorbent dosage, shaking speed, pH, initial concentration, and temperature were studied. In addition, the isotherms, thermodynamics, and kinetics of methylene blue adsorption were also presented, giving theoretical support for the solid–liquid adsorption research and treatment of methylene blue wastewater.

2. Experimental

2.1. Materials

Zirconium chloride ($ZrCl_4$), terephthalic acid ($C_8H_6O_4$), and 2-aminoterephthalic acid ($C_8H_7NO_4$), methylene blue ($C_{16}H_{18}ClN_3S{\cdot}3H_2O$) were obtained from Shanghai Aladdin. *N*,*N*-Dimethylformamide, acetic acid, ferric sulfate, hydrogen peroxide, ethanol, and sodium hydroxide were purchased from Sinopharm Chemical Reagent (Shanghai, China).

2.2. Methods

2.2.1. Analysis method

The concentration of methylene blue was measured with a visible spectrophotometer (UV-1800PC, Shanghai MAPADA Instrument Co., Ltd., China) at 665 nm. The standard curve of the concentration of methylene blue (y, mg/L) vs. absorbance (x) is $y = 4.8160x - 0.0057$, the range of x is 0–5.0, and the determination coefficients of the curve is 0.9995.

2.2.2. Preparation of the MOFs

UiO-66 and UiO-66-NH_2 were synthesized by a solvothermal method with some modifications to the previously reported procedure. The detailed procedure of UiO-66 or UiO-66-NH_2 is as follows: 0.22 g of terephthalic acid (or 0.24 g of 2-aminoterephthalic acid), 0.30 g of zirconium chloride, 11.71 g of acetic acid, and 61.76 g of *N*,*N*-dimethylformamide were added sequentially into a 100 mL conical flask. The molar ratio of the above four raw materials is 1:1:150:650. After shaking, the flask was sonicated for half an hour. Subsequently, the dissolved sample was sent to a reaction kettle and crystallized at 120°C for 24 h. After the temperature dropped to room temperature, a solid was obtained after centrifugation and washed with *N*,*N*-dimethylformamide and ethanol for three times. Each wash was magnetically stirred for half an hour and then centrifuged. After washing, the desired product was dried at 110°C for 10 h in a vacuum oven. The dried product was then naturally cooled, ground, and sieved through a 100-mesh screen, and stored in desiccators for use.

2.3. Characterization

The XRD data of the sample was measured by X-ray diffraction spectroscope (Rigaku UItimaIV, Japan) with Cu Kα radiation. The FT-IR spectra of the sample in the frequency range of 4,000–400 cm^{-1} was recorded by using an infrared spectrometer (Thermo Fisher Nicolet iS10, USA). The surface morphology of the sample was studied by

SEM (ZEISS SUPRA 55, German). BET specific surface area and pore size were characterized on an automatic surface analyzer (Micromeritics ASAP 2460, USA).

2.4. Adsorption experiment

The batch adsorption experiments were performed by adding different mass of MOFs with 20 mL of methylene blue aqueous solution at the specified concentration and pH in a 100 mL flask. The flasks were then immersed in a water bath oscillator at a constant shaking speed and temperatures. The samples were taken and separated by centrifuge. The concentration of methylene blue was measured by a visible spectrophotometer. The adsorption capacity of methylene blue on MOFs at a given time (q_t, mg/g) and at the state of equilibrium (q_e, mg/g), and the percentage removal of methylene blue, R_e (%), were determined as follows:

$$q_t = \left(C_0 - C_t\right) \times \frac{V}{m} \tag{1}$$

$$q_e = \left(C_0 - C_e\right) \times \frac{V}{m} \tag{2}$$

$$R_e\left(\%\right) = 100 \times \frac{\left(C_0 - C_e\right)}{C_0} \tag{3}$$

where C_0 is the initial concentration (mg/L), C_t is the concentration at a specific time (mg/L), C_e is the concentration at the state of equilibrium (mg/L), m is the weight of the used adsorbent (g), and V is the solution volume (L).

2.5. Regeneration study

The methylene blue recovery experiments were according to the following procedure. Before desorption, the following parallel adsorption experiments were carried out: UiO-66-NH_2, 0.06 g, and 20 mL of methylene blue solution with initial concentrations 50 mg/L was placed into flask. The flask was shaken at 210 rpm and 318.15 K for 5 h, and the adsorption reached equilibrium. After the adsorption of methylene blue, the UiO-66-NH_2 loaded with methylene blue was dried. Then 0.06 g of UiO-66-NH_2 loaded with methylene blue was added in 100 mL flask with 25 mL ethanol. The mixture was sonicated for an hour and separated by centrifuge. The adsorbent was then sonicated for an hour with 25 mL of 1:1 ethanol and distilled water twice. After centrifugal separation, the adsorbent was dried for 10 h in a vacuum oven at 90°C. The recovered UiO-66-NH_2 was used again as an adsorbent to adsorb methylene blue from an aqueous solution.

3. Results and discussion

3.1. Characterization of the adsorbents

3.1.1. X-ray diffraction

The powder XRD spectrum of UiO-66 and UiO-66-NH_2 are displayed in Fig. 2. The characteristic peaks of UiO-66 are 2θ = 7.48°, 8.62°, 12.14°, 14.22°, 17.14°, 22.30°, 25.78°, and 33.16°, corresponding to (111), (002), (022), (113), (004), (115), (224), and (137) crystal planes, respectively [34,35]. UiO-66 has obvious diffraction peaks at these eight characteristic positions, and it is in good agreement with the theoretical spectrum. The XRD pattern of the synthesized UiO-66-NH_2 agrees well with the characteristic reflection peaks of the UiO-66 crystal pattern, indicating that the successful preparation of UiO-66-NH_2.

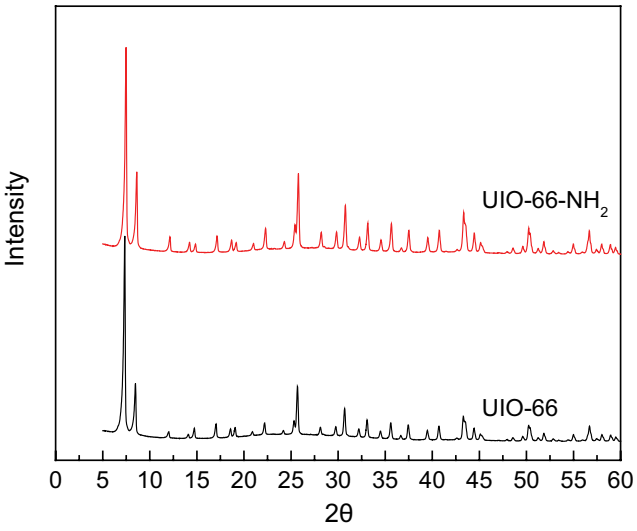

Fig. 2. XRD patterns of UiO-66 and UiO-66-NH_2.

3.1.2. Fourier-transform infrared spectroscopy

The FT-IR spectrum of UiO-66, UiO-66-NH_2 before and after adsorption, and UiO-66-NH_2 after the fourth adsorption are exhibited in Fig. 3. For UiO-66, the characteristic peak at 1,658 cm^{-1} is related to the stretching vibration of C=O in terephthalic acid, revealing that the metal is coordinated to the organic fraction of terephthalic acid [36]. The vibration at 1,587 cm^{-1} corresponds to the asymmetric stretching vibration bands of O–C–O in the ligand, which indicates the presence of carboxylic acid groups in the framework. The vibrations at 1,506 and 1,398 cm^{-1} are attributed to the C=C double bond of the benzene ring. The peaks at 814, 746, and 667 cm^{-1} are the vibrations of the O–H bond and C–H bond in the ligand. Furthermore, the peak at 553 cm^{-1} in the low-frequency region is the asymmetric stretching of Zr-(OC). For the spectrum of UiO-66-NH_2, the –NH_2 functional group exhibits some characteristic absorption bands. The C–N stretching vibration was observed at 1,255 cm^{-1}, while N–H wagging was found at 769 cm^{-1}. These FTIR results verify the existence of –NH_2 groups in UiO-66-NH_2. After adsorption, the infrared spectrum of UiO-66-NH_2 remains almost unchanged.

3.1.3. Scanning electron microscopy

The SEM images of the UiO-66, UiO-66-NH_2 before and after adsorption at 50,000 magnification times are exhibited in Fig. 4, which indicated the two MOFs were crystallized well. It can be clearly seen from Fig. 4a that the prepared

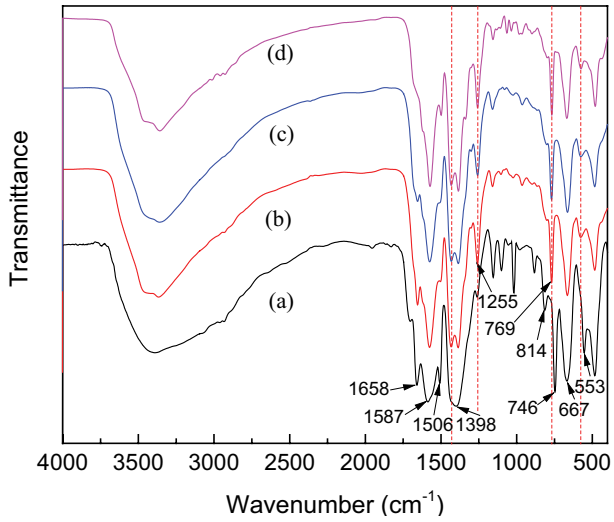

Fig. 3. FT-IR spectroscopy of (a) UiO-66, (b) UiO-66-NH_2, (c) UiO-66-NH_2 after adsorption, and (d) UiO-66-NH_2 after fourth adsorption.

UiO-66 particles have a standard octahedral morphology, smooth, and clear edges, complete structure, good dispersion between the particles, and almost no agglomeration. The size of the particles is about 400 nm. The crystal structure of UiO-66-NH_2 shown in Fig. 4b is similar to UiO-66, but its particle size is about 200 nm, which is smaller than UiO-66. After adsorption, the structure of UiO-66-NH_2 doesn't collapse but remains almost unchanged, indicating its good stability.

3.1.4. Nitrogen adsorption–desorption

The N_2 adsorption/desorption isotherms of the samples are shown in Fig. 5. It can be seen from the figure that the N_2 adsorption/desorption isotherms of the two MOFs samples are type I isotherms and the adsorption take place at relatively low pressure (P/P_0), which is the characteristic adsorption type of microporous materials. As shown in Table 1, compared with UiO-66, the BET surface area and pore volume of UiO-66 after functionalization with amino groups are both reduced, which may be due to the volume occupied by the additional functional groups leading to a partial reduction in the pore space. The average pore diameters of UiO-66 and UiO-66-NH_2 are comparable, and both less than 2 nm. The BET surface areas of UiO-66 and UiO-66-NH_2 are 1,394.4 and 1,052.0 m^2/g, respectively, which are larger than that reported in the literature [36–38]. UiO-66 and UiO-66-NH_2 have a ratio of micropore volume to total pore volume greater than 70%, which are outstanding adsorbent for adsorption. After adsorption, the surface area, total pore volume, and average pore diameter of UiO-66-NH_2 increase slightly.

3.2. Factors affecting adsorption

3.2.1. Effect of adsorbent dosage

The effect of adsorbent dosage on the adsorption was carried out by varying the dosage of two adsorbents from

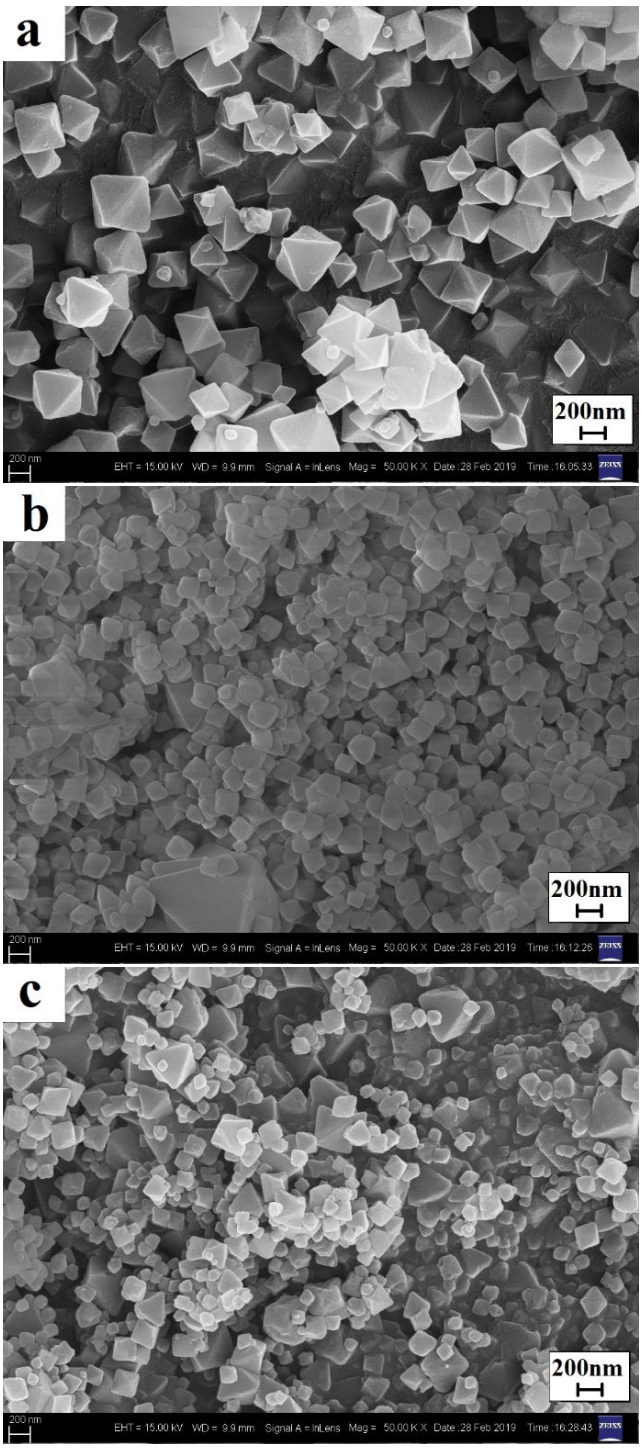

Fig. 4. SEM images of (a) UiO-66, (b) UiO-66-NH_2, and (c) UiO-66-NH_2 after adsorption

0.02 to 0.12 g for mixing with 20 mL of 50 mg/L of methylene blue solutions shaken at 210 rpm and 298.15 K for 5 h. The percent removal of methylene blue was obtained, and the results are displayed in Fig. 6a. As shown in this Fig. 6, the adsorption performance of UIO-66-NH_2 is better than of UIO-66 in the range of the adsorbent used. It may be due to the presence of an electron-donating group amino group

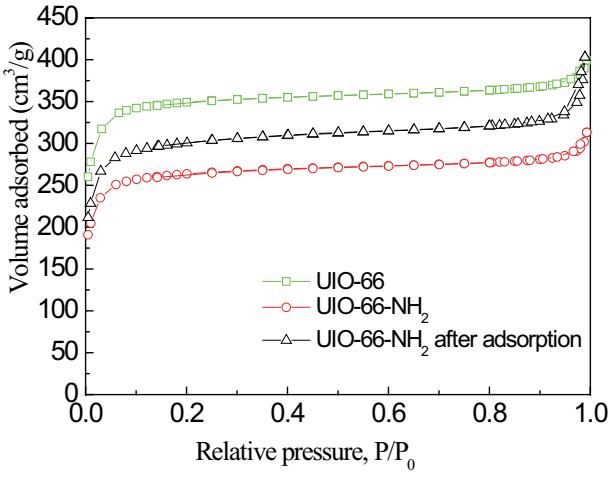

Fig. 5. N_2 adsorption and desorption isotherm of the UiO-66, UiO-66-NH_2 before and after adsorption.

on UIO-66-NH_2, which enhances the electrostatic attraction between the cationic dye (methylene blue) and the negatively charged surface of adsorbent. In addition, the molecular structure and size of methylene blue were calculated by Gaussian 16 using b3lyp/6–31+g(d,p) method and shown in Fig. 1. The size of methylene blue is less than the average pore diameter of UiO-66 or UiO-66-NH_2, which indicates that methylene blue molecules can enter the pores of the adsorbent and be adsorbed in the pores. Furthermore, the percentage removal of methylene blue is promoted with the increase of the UIO-66-NH_2 dosage because of the more active sites for adsorption. Therefore, the UIO-66-NH_2 was selected to adsorb methylene blue from an aqueous solution in the further study.

3.2.2. Effect of shaking speed

The effect of shaking speed was studied at three different shaking speeds from 160 to 260 rpm with 20 mL of 50 mg/L methylene blue solution containing 0.06 g UIO-66-NH_2 at 298.15 K. The adsorption capacity of methylene blue vs. time at different shaking speeds are plotted and displayed in Fig. 6b. It can be seen from the figure that the adsorption rate of methylene blue on UIO-66-NH_2 increases with an increase of shaking speed from 160 to 210 rpm and then is found to remain substantially constant with the further increase of the shaking speed. The above results may be that the increase in the mixing degree reduces the thickness of the boundary layer around the adsorbate particles [39]. When the mixture was shaken, the adsorbed solid particles quickly move into the solution, which makes the concentration of methylene blue near the surface of the solid particles and approach the total concentration [40]. As the shaking speed was changed from 160 to 210 rpm, the external mass transfer rate of methylene blue increase. However, the external mass transfer rate remains constant by further ascending the shaking speed, which indicates that the external diffusion resistance keeps constant. Hence, the shaking speed was set at 210 rpm in further studies.

3.2.3. Effect of pH

The pH of the solution is a key variable for the adsorption of dye on MOFs, and it changes the charge distribution on the surface of the adsorbent and affects the interaction between the adsorbent and the dye [1]. The experiments were investigated in the pH range of 1–10 with 20 mL of 50 mg/L of methylene blue solution and 0.06 g UIO-66-NH_2 at 210 rpm and 298.15 K for 5 h. The equilibrium adsorption capacity of methylene blue was obtained, and the results are presented in Fig. 6c. It is obvious that the equilibrium adsorption capacity of methylene blue increases from 4.23 to 10.10 mg/g when the solution pH was increased from 1 to 6. Then, the pH has no significant effect over the range 6–10, and the equilibrium adsorption capacity of methylene blue varies between 10.06 and 10.35 mg/g. This can be explained by the protonation of the amino group of the UIO-66-NH_2 at low pH, forming a new substance that competes with the cationic methylene blue, reducing the interaction between methylene blue and the more positive adsorbent, and thereby depressing the adsorption capacity [41]. Conversely, the surface of UIO-66-NH_2 generates a lot of negative charges by raising the pH, thus enhancing the electrostatic interaction with methylene blue and improving the adsorption capacity. Thereby, the optimal pH range is 6–10.

3.2.4. Effect of initial concentration

The effect of the initial concentration of methylene blue (50–300 mg/L) on the removal (%) was carried out as follows: UIO-66-NH_2, 0.06 g, and 20 mL of methylene blue solution

Table 1
Physical property of UiO-66, UiO-66-NH_2 before and after adsorption

Parameters	UiO-66	UiO-66-NH_2	UiO-66-NH_2 after adsorption
BET surface area, S_{BET} (m^2/g)	1,394.4	1,052.0	1,193.0
Micropore area, S_{micro} (m^2/g)	1,272.0	933.1	1,025.2
External surface area, S_{ext} (m^2/g)	122.4	118.9	167.7
Micropore volume, V_{micro} (cm^3/g)	0.4866	0.3558	0.3917
Mesopore volume, V_{meso} (cm^3/g)	0.1311	0.1285	0.2317
Total pore volume, V_T (cm^3/g)	0.6177	0.4843	0.6234
Average pore diameter, APD (nm)	1.7718	1.8415	2.0903

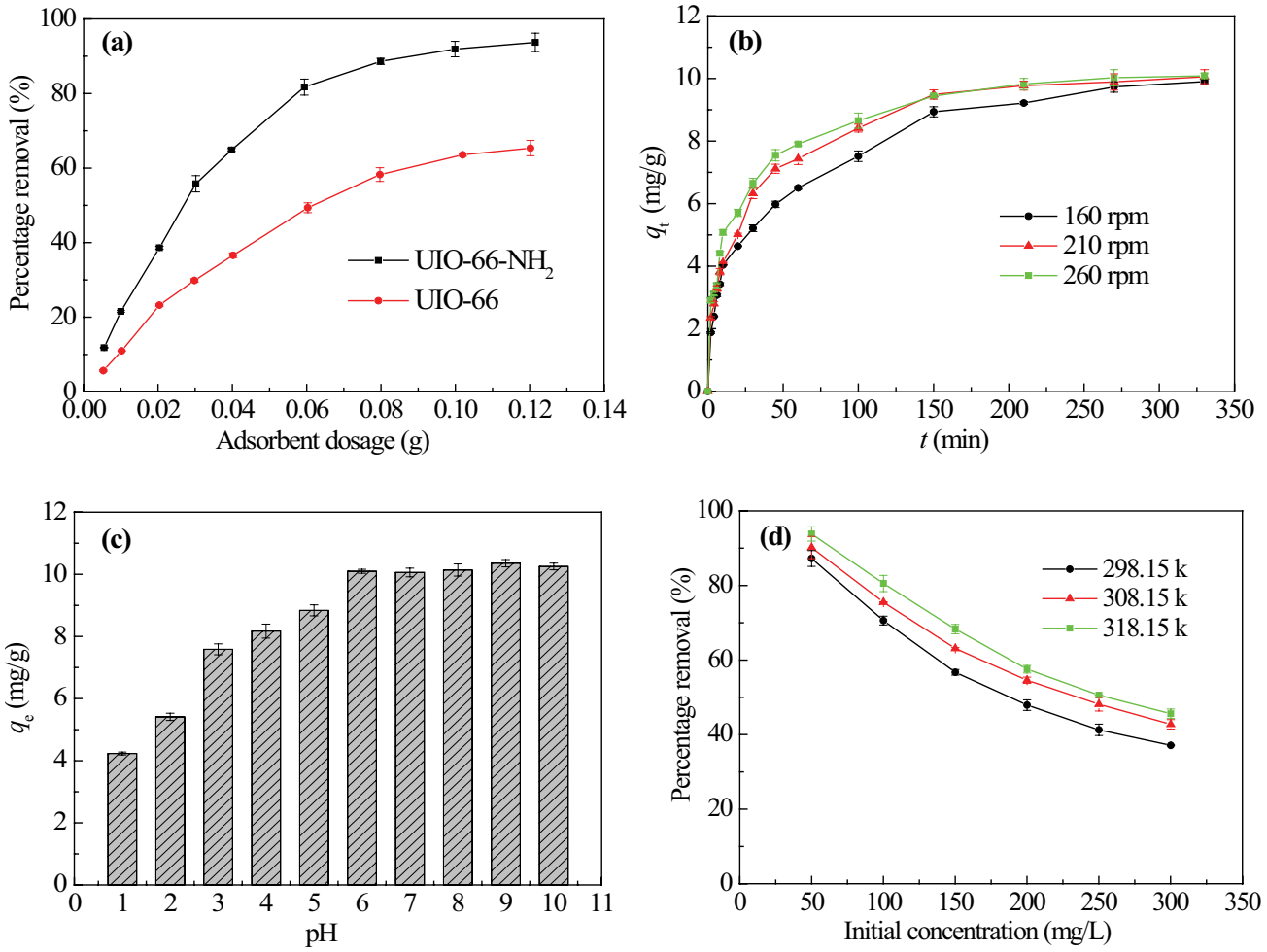

Fig. 6. Effect of (a) adsorbent dosage, (b) shaking speed, (c) pH, and (d) initial concentration on the adsorption of methylene blue.

with different initial concentration were put into flask. The solutions were then shaken at 210 rpm and temperatures of (298.15, 308.15, and 318.15 K) for 5 h. The samples were analyzed and the equilibrium concentrations of methylene blue were determined. The equilibrium adsorption capacity and the percentage removal of methylene blue were both obtained and shown in Fig. 6d. It can be seen from the figure that the percentage removal of methylene blue by UIO-66-NH_2 gradually decreases with the increase of the initial concentration from 50 to 300 mg/L. This is because the active sites provided by the UIO-66-NH_2 is limited when the amount of the used adsorbent is fixed. Afterwards, these active sites tend to be saturated, losing the ability to adsorb more molecules of methylene blue at higher concentrations. It can also be seen from the figure that the percentage removal of methylene blue enhances with rising the temperature from 298.15 to 318.15 K at the same initial concentration, which indicates that the increase in temperature is favorable for adsorption, that is, the adsorption process is an endothermic process.

3.3. Adsorption isotherms

Adsorption isotherm is helpful to evaluate the adsorption ability of adsorbent, and can be further used to clarify the interaction between adsorbent and adsorbate. The adsorption isotherms of methylene blue on UIO-66-NH_2 were performed at three different temperatures from 298.15 to 318.15 K. The specific experimental conditions were shown in section 3.2.4 (Effect of initial concentration), and three adsorption equilibrium curves at different temperatures were acquired and displayed in Fig. 7, which were the plots of q_e against C_e.

The adsorption isotherms data were analyzed by using several models, such as Langmuir (Eq. (4)), Freundlich (Eq. (5)), Redlich–Peterson (Eq. (6)), Sips (Eq. (7)), and Temkin (Eq. (8)) models [42]. The non-linear forms of the five models were listed as follows:

$$q_e = \frac{q_m K_L C_e}{1 + K_L C_e} \tag{4}$$

$$q_e = K_F C_e^{1/n_F} \tag{5}$$

$$q_e = \frac{K_{RP} C_e}{1 + \alpha_{RP} C_e^{\theta}} \tag{6}$$

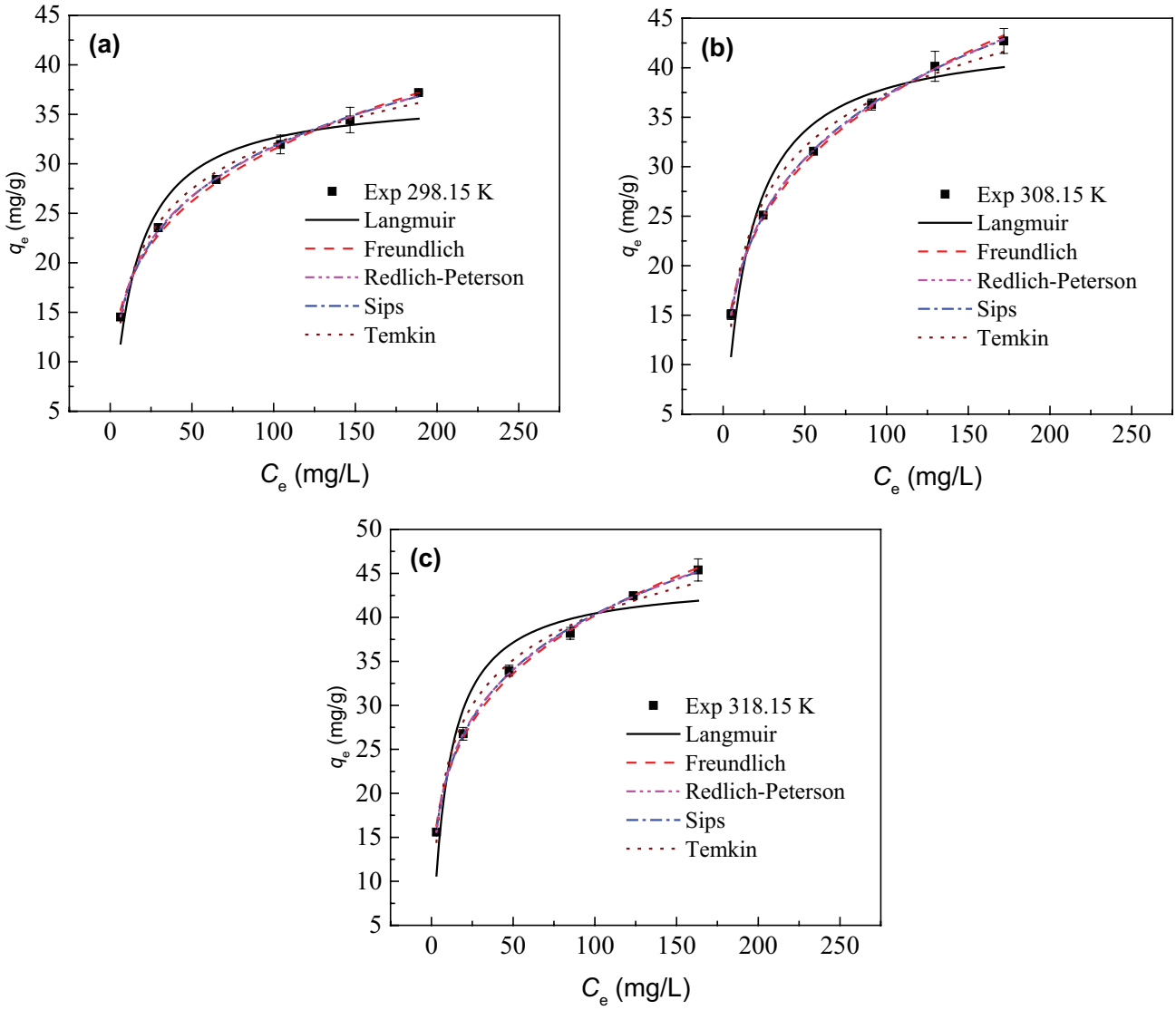

Fig. 7. Experimental data of adsorption isotherm and non-linear adjustments of the isotherm models at the temperature of (a) 298.15 K, (b) 308.15 K, and (c) 318.15 K.

$$q_e = \frac{q_m K_S C_e^{1/n_S}}{1 + K_S C_e^{1/n_S}} \tag{7}$$

$$q_e = \frac{RT}{\beta_T} \ln\left(\alpha_T \cdot C_e\right) \tag{8}$$

where q_m (mg/g) is the maximum adsorption capacity of methylene blue onto the adsorbent surface, and K_L (L/mg) is the Langmuir constant. K_F ((mg/g)/(mg/L)$^{1/n}$) and n_F are the Freundlich constants. K_{RP} (L/g), α_{RP} ((L/mg)$^{\theta}$), and θ (≤1) are the Redlich–Peterson constants. K_S ((L/mg)$^{1/n_S}$) and n_S is the Sips constants. α (L/mg) and β_T (J/mol) are the Temkin constants. R is the gas constant (8.314 J/mol K), and T is the absolute temperature (K). The non-linear method was used to determine the best-fit adsorption isotherm model by judging the determination coefficient (R^2) and the chi-square value (χ^2). The expression of the chi-square test is as follows [43,44]:

$$\chi^2 = \sum \frac{\left[\left(q_{e,\exp} - q_{e,\text{cal}}\right)\right]^2}{q_{e,\text{cal}}} \tag{9}$$

where the subscripts "exp" and "cal" represent the experimental and calculated values, respectively. For the non-linear fitting, it is not reasonable to use only one parameter of the correlation coefficient to determine the best-fit adsorption isotherm. Nevertheless, the chi-square test is a better method to determine the best-fit model [43]. If the calculated value from the model agrees well with the experimental data, the value of χ^2 will be small and close to zero. A higher χ^2 reveals a vast deviation between the experiment and the model. Therefore, it is feasible to check the best-fit adsorption isotherm model by chi-square

analysis. The five non-linear forms of adsorption isotherms models were fitted to experimental data by using OriginPro 2015 with Levenberg–Marquardt algorithm and displayed in Fig. 7, while the correlated parameters were shown in Table 2.

As shown in Table 2, the lowest R^2 and the highest χ^2 at each temperature indicate that the adsorption of methylene blue on UIO-66-NH_2 is not well-described by the Langmuir isotherm. The remaining four models fit well the experimental data at three different temperatures because of the higher values of R^2 (≥0.985) and lower values of χ^2 (≤0.25). On the basis of the highest values of $R^2 \geq 0.9985$ and the lowest values of $\chi^2 \leq 0.0113$, we can conclude that the Redlich–Peterson model is the best-fit isotherm model for the adsorption of methylene blue onto UIO-66-NH_2.

Redlich–Peterson model contains features of both Langmuir and Freundlich isotherms, which forms a hybrid adsorption mechanism and can be used either in multilayer and monolayer adsorption [45]. This model can well describe the adsorption isotherms in a wide concentration range of adsorbate. The exponent θ of the Redlich–Peterson model ranges from 0 to 1, and the value of exponent indicates that Redlich–Peterson model exhibits different models: Langmuir (θ = 1), Freundlich ($0 < \theta < 1$, $K_{RP} \gg 1$, and $\alpha_{RP} \gg 1$), and Henry's law (θ = 0). It can be clearly seen from Table 2 that Freundlich model can better describe the adsorption isotherm than Langmuir under different temperatures according to the values of θ, K_{RP}, and α_{RP}. The adsorption isotherm modeling demonstrates that the adsorption of methylene blue on UIO-66-NH_2 occurs in multilayers [46].

The maximum adsorption capacity of methylene blue on UIO-66-NH_2 obtained in the adsorption isotherms condition is 45.4 mg/g at methylene blue concentration of 300 mg/L and 318.15 K. The comparison of the maximum adsorption capacity with previously adsorbents is displayed in Table 3. It can be seen that the adsorption capacity of methylene blue onto UIO-66-NH_2 is good and lies in the middle between different adsorbents, which indicates that the UIO-66-NH_2 is an excellent adsorbent.

Table 2
Isotherm parameters for the adsorption of methylene blue on UIO-66-NH_2

Models	Parameters	T (K)		
		298.15	308.15	318.15
Langmuir	K_L (L/mg)	0.0737	0.0677	0.1023
	q_m (mg/g)	37.03	43.51	44.40
	R^2	0.9149	0.9087	0.88285
	χ^2	1.1280	2.2431	3.1773
Freundlich	K_F ((mg/g)/(mg/L)$^{1/n_F}$)	3.7955	3.4950	3.8622
	n_F	9.36	9.92	12.20
	R^2	0.9951	0.9978	0.9968
	χ^2	0.0668	0.0386	0.0647
Redlich–Peterson	K_{RP} (L/mg)	13.25	21.75	35.57
	α_{RP} ((L/mg)$^{\theta}$)	1.13	1.87	2.54
	θ	0.78	0.74	0.77
	R^2	0.9985	0.9995	0.9988
	χ^2	0.0101	0.0040	0.0113
Sips	K_S ((L/mg)$^{1/n_S}$)	0.0981	0.0726	0.0910
	q_m (mg/g)	89.53	129.93	133.51
	n_S	2.67	2.69	2.95
	R^2	0.9974	0.9996	0.9984
	χ^2	0.0191	0.0031	0.0162
Temkin	α_T (L/mg)	1.3299	1.2153	2.2777
	β_T (J/mol)	378.96	328.83	356.23
	R^2	0.9918	0.9849	0.9854
	χ^2	0.0819	0.2522	0.2508

3.4. Adsorption thermodynamics

Thermodynamic adsorption studies play a significant role in illustrating adsorptive mechanisms and the energy change of adsorbents before and after adsorption. The thermodynamic parameters for the adsorption of methylene blue onto UIO-66-NH_2 include the Gibbs energy change (ΔG), the enthalpy change (ΔH), and the entropy change (ΔS). These parameters were calculated using the following equations [47,48]:

$$\Delta G = -RT \ln K_e \tag{10}$$

$$\ln K_e = -\frac{\Delta H}{RT} + \frac{\Delta S}{R} \tag{11}$$

where K_e is the dimensionless thermodynamic equilibrium constant, which is determined through converting the units of the best-fit isotherm model Redlich–Peterson constant (K_{RP}) in our work [49]. The process obtaining the dimensionless K_e is as follows:

$$K_e = \frac{K_{RP} M_{adsorbate} \left[\text{Adsorbate}\right]^0}{\gamma} \tag{12}$$

where $M_{adsorbate}$ is the molecular mass of adsorbate (g/mol), $[\text{Adsorbate}]^0$ is the standard concentration of adsorbate (mol/L), and γ is the adsorbate activity coefficient. The molecular mass of methylene blue is 319.86 g/mol, and the activity coefficient and the standard concentration were assumed to be 1 and 1 mol/L, respectively.

Table 3
Maximum adsorption capacities of methylene blue for different adsorbents

Adsorbents	q_{max} (mg/g)	References
Bituminous coal	2.02	[22]
Kenaf fiber char	22.7	[59]
Waste apricot activated carbon	102.0	[60]
Chitosan-graphite oxide	64.9	[61]
Hazelnut shell activated carbon	8.8	[62]
Chitosan/PVA composite	52.9	[30]
Magnetic biochar composite	24.8	[63]
UIO-66-NH_2	45.4	Our work

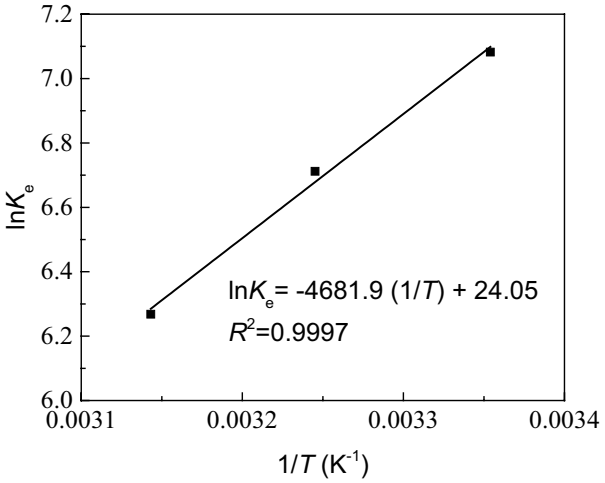

Fig. 8. Plot of $\ln K_e^0$ vs. $1/T$.

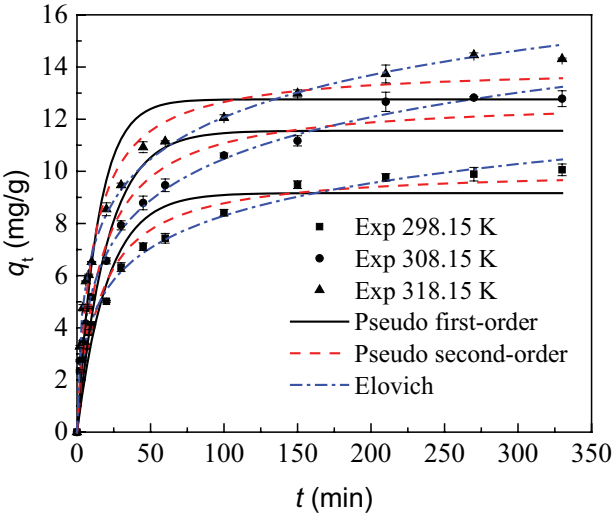

Fig. 9. Experimental data of adsorption kinetics and non-linear fitting of kinetics models.

The Gibbs energy change (ΔG) was directly determined from Eq. (10), and the enthalpy change (ΔH), and the entropy change (ΔS) were calculated from the slope and intercept of a plot of $\ln K_e$ vs. $1/T$ which is displayed in Fig. 8. The results of the thermodynamic studies are listed in Table 4. The negative values of ΔG demonstrate the spontaneous adsorption process [50]. The positive value of ΔS reveals that the adsorption of methylene blue onto UIO-66-NH_2 is entropy driven rather than enthalpy driven [51]. Moreover, the positive value of ΔH verifies the endothermic nature of the methylene blue adsorption on UIO-66-NH_2 and increasing the temperature improves adsorption.

3.5. Adsorption kinetics

The adsorption kinetics can demonstrate the adsorption rate of adsorbent onto adsorbent and determine the equilibrium time [52]. The kinetic parameters obtained from the kinetic data modeling are of great significance for estimating the adsorption rate and give critical information for process design to determine the adsorption mechanism and possible rate-limiting steps. The experiments of adsorption kinetics were investigated as follows: 0.06 g of UIO-66-NH_2 was mixed with 20 mL of 50 mg/L methylene blue solution and put into 100 mL flask. The mixture was shaken at 210 rpm and three different temperatures from 298.15 to 318.15 K, respectively. The adsorption capacity of methylene blue on UIO-66-NH_2, q_t (mg/g) vs. time are displayed in Fig. 9. It can be seen from the Fig. 9 that the rate of adsorption and equilibrium adsorption capacity both promote with increasing temperature. The result further exhibits that the adsorption of methylene blue onto UIO-66-NH_2 is exothermic, which is aligned with the thermodynamics of adsorption.

Table 4
Thermodynamic parameters for the adsorption of methylene blue

T (K)	ΔG (kJ/mol)	ΔH (kJ/mol)	ΔS (J/mol·K)
298.15	–20.70		
308.15	–22.67	38.93	199.96
318.15	–24.70		

Three kinetic models were selected to fit the kinetic data, which are pseudo-first-order, pseudo-second-order, and Elovich kinetic models, described by Eqs. (13)–(15), respectively [46,53]:

$$q_t = q_e\left[1-\exp\left(-k_1 t\right)\right] \tag{13}$$

$$q_t = \frac{k_2 q_e^2 t}{1+k_2 q_e t} \tag{14}$$

$$q_t = \frac{1}{\beta}\ln\left(1+\alpha\beta t\right) \tag{15}$$

where k_1 (min^{-1}) and k_2 (g/mg min) are the rate constant of the pseudo-first-order and second-order models, respectively; α (g/mg min^2) and β (mg/g min) are Elovich constants, which stand for the initial adsorption rate and the desorption coefficient, respectively.

The adsorption kinetics data was analyzed by non-linear curve fitting analysis method using Origin 2015 to fit the selected three kinetic models by the determination coefficient (R^2) and the chi-square value (χ^2). In addition, q_e in the chi-square (χ^2) of Eq. (9) needs to be substituted by q_t. The fitting results are displayed in Fig. 9 and the model parameters were shown in Table 5. From Fig. 9 and Tables 5, it seems that the pseudo-first-order model is not suitable to describe the experimental data due to the lowest values of R^2 (0.9119–0.9140) and highest values of χ^2 (4.04–5.61) at three different temperatures. The pseudo-second-order and Elovich kinetic models are well-fitted to experimental data. The equilibrium adsorption capacities obtained from pseudo-second-order model are very close to experimental values, presenting

the high R^2 (0.9698–0.9742) and low χ^2 values (1.19–1.85). Hence, the adsorption kinetic data of methylene blue on UIO-66-NH_2 is best fitted by Elovich model because of the highest values of R^2 (0.9929–0.9961) and lowest values of χ^2 (0.12–0.20). The Elovich model is based on the assumption that the adsorbent surface is heterogeneous in energy and that the adsorption kinetics is independent of the desorption or interaction between adsorbed species at low surface coverage [54].

In order to determine the rate control steps of the adsorption process, the intraparticle diffusion model proposed by Weber and Morris was further used to fit to the experimental data of adsorption kinetics, described by Eq. (16) [54]. The model presumes that the adsorption occurs through the diffusion of the adsorbed molecules into the pores of the adsorbent:

$$q_t = k_{id} t^{1/2} + C \tag{16}$$

where k_{id} (mg/g $min^{-0.5}$) and C (mg/g) are the intraparticle diffusion constants. The plots of q_t vs. $t^{1/2}$ are exhibited in Fig. 10, and the values of k_{id}, C_i, and R^2 are shown in Table 6. If q_t is linear with $t^{1/2}$ and passes through the origin, the rate control step is only due to intraparticle diffusion. Otherwise, there are other rate controls together with intraparticle diffusion.

Fig. 10 indicates that there are three different stages of linearity for the adsorption of methylene blue on UIO-66-NH_2 at each temperature, presenting that the adsorption process is governed by a multi-step control [55]. The first stage, starting from the origin, is the external diffusion of methylene blue through the solution to the external surface of UIO-66-NH_2, or the boundary layer diffusion of methylene blue [56]. The big k_{id} values in this stage reveal that the rate of adsorption is fast. The second stage is in regard to the gradual adsorption, where intraparticle diffusion is the rate-limiting step. The third stage is ascribed to the final equilibrium stage. In this stage, the intraparticle diffusion commences to slow down due to the greatly dilute concentration of methylene blue left in the solution. The intercept value, C, represents the thickness of the boundary layer [57]. The C values of three stages at three different temperatures are arranged in the following order $C_3NC_2NC_1$, listed in Table 6. The results reveal that the smaller external diffusion resistance at first stage owning to the higher vacant adsorption sites. In addition, the straight lines of the other two stages deviate from the origin, which implies that the rate control step isn't only on account of the intraparticle diffusion [58]. The multiple natures of the plots at different temperatures can be attributed to the boundary layer diffusion (the first stage) and the intraparticle diffusion (the other two stages).

Table 5
Kinetic model parameters for the adsorption of methylene blue

Models	Parameters	T (K)		
		298.15	308.15	318.15
Pseudo-first-order	$q_{e,exp}$ (mg/g)	10.06	12.83	12.46
	k_1 (min^{-1})	0.0483	0.0484	0.0710
	$q_{e,cal}$ (mg/g)	9.17	11.55	12.76
	R^2	0.9140	0.9126	0.9119
	χ^2	5.0238	5.6096	4.0417
Pseudo-second-order	k_2 (g/mg min)	0.0065	0.0051	0.0067
	$q_{e,cal}$ (mg/g)	10.10	12.79	14.01
	R^2	0.9698	0.9703	0.9742
	χ^2	1.7285	1.8498	1.1916
Elovich	α	1.7344	2.0791	4.0684
	β	0.5507	0.4298	0.4278
	R^2	0.9929	0.9961	0.9954
	χ^2	0.1973	0.1261	0.1248

3.6. Adsorption mechanism

The above results indicate UiO-66-NH_2 has excellent adsorption performance for methylene blue. The possible adsorption mechanism of methylene blue on UiO-66-NH_2 is exhibited in Fig. 11. It can be seen from the structure of UiO-66-NH_2 that there are two functional groups viz.

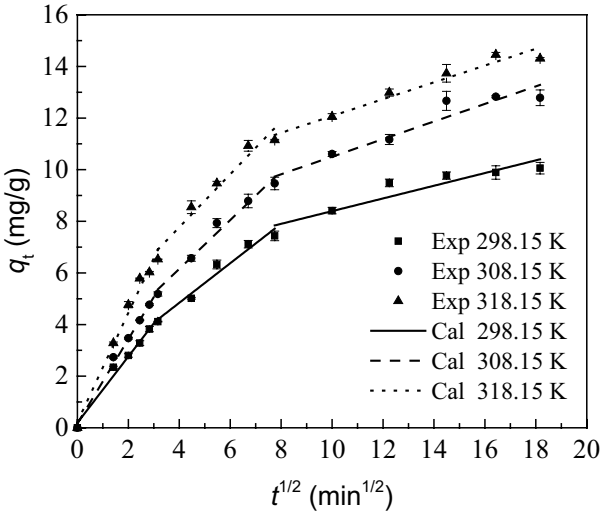

Fig. 10. Intraparticle diffusion plots for methylene blue adsorption at different temperatures.

Table 6
Parameters of intraparticle diffusion model

Parameters	T (K)		
	298.15	308.15	318.15
$k_{id,1}$ (mg/g $min^{0.5}$)	1.2838	1.6326	2.1122
C_1 (mg/g)	0.1914	0.1625	0.2248
R^2	0.9841	0.9933	0.9839
$k_{id,2}$ (mg/g $min^{0.5}$)	0.7664	0.9461	1.0255
C_2 (mg/g)	1.7761	2.3713	3.6684
R^2	0.9644	0.9802	0.9563
$k_{id,3}$ (mg/g $min^{0.5}$)	0.2459	0.3406	0.3257
C_3 (mg/g)	5.9346	7.0972	8.8225
R^2	0.8773	0.9220	0.9563

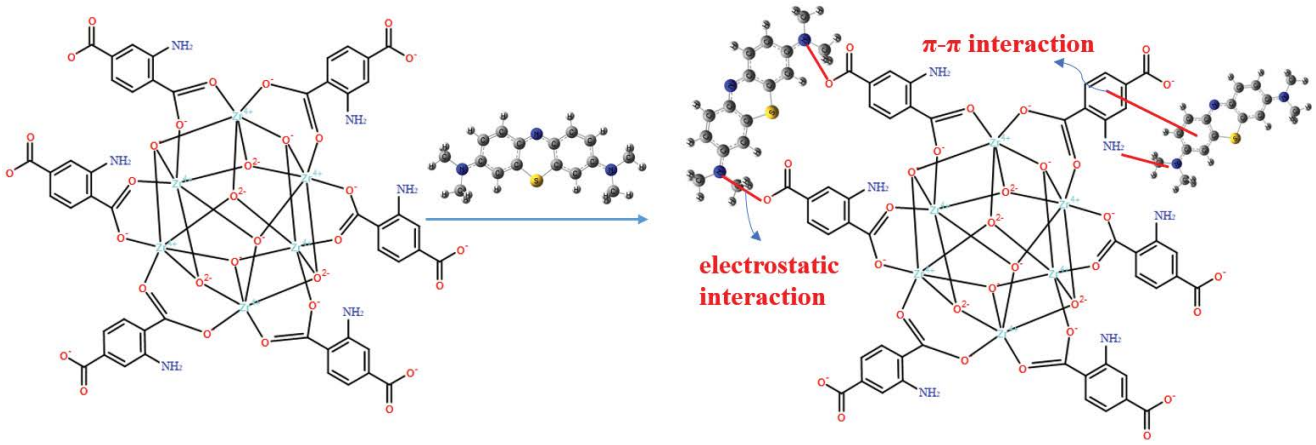

Fig. 11. Adsorption mechanism for methylene blue onto UIO-66-NH_2.

carboxylic and amino groups. Moreover, there are a lot of benzene rings on the absorbent. Therefore, the adsorption might be occurred by three mechanisms: (1) electrostatic interaction between electron-rich nitrogen and nitrogen, (2) electrostatic interaction between electron-rich oxygen and nitrogen, (3) and π–π interaction between the surface of UiO-66-NH_2 and methylene blue [29].

3.7. Regeneration study

From an economic perspective, the regeneration and reusability of the adsorbents is a vital element in assessing the performance of adsorption materials. In this work, the desorption of methylene blue from UIO-66-NH_2 was evaluated with ethanol as eluents, and five adsorption–desorption cycles were performed. The results are exhibited in Fig. 12. As can be seen form Fig. 12, the removal of methylene blue declines slightly in each cycle, but still has a high adsorption capacity, which demonstrates that UIO-66-NH_2 has outstanding regeneration and recyclability. Thus, UIO-66-NH_2 can be employed as a cost-effective and environmentally friendly adsorbent for the methylene blue removal from wastewater.

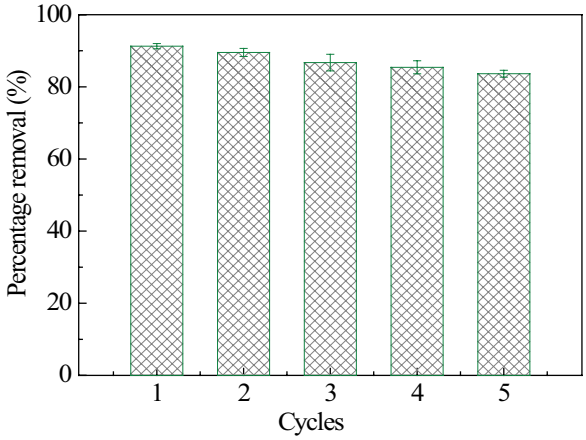

Fig. 12. Adsorption cycles performance of UIO-66-NH_2 for removal methylene blue.

4. Conclusions

In this work, two Zr-containing MOFs UiO-66 and UiO-66-NH_2 were synthesized and characterized by XRD, FT-IR, SEM, and BET, which were further used as an adsorbent for the methylene blue removal from aqueous solution. Even though, the porosity and surface area of the UiO-66-NH_2 were less than that of the original UiO-66, its adsorption capacity for methylene blue improves remarkably after the functionalization of free amino groups, which can be attributed to electrostatic attraction between the cationic dye and the negatively charged surface of adsorbent. The adsorption equilibrium data of methylene blue by UiO-66-NH_2 was best fitted by the Redlich–Peterson model. The Elovich model can be favorably applied to describe the adsorption kinetics. The adsorption process is an exothermic and of the multilayer variety. Thermodynamic parameters such as ΔG, ΔH, and ΔS were calculated, revealing that the adsorption endothermic and spontaneous. Furthermore, the adsorbent UiO-66-NH_2 can be easily regenerated and recycled by ethanol as eluent, and the adsorption capacity was only reduced by 5% after five cycles. Hence, UiO-66 functionalized with basic site can be employed as an environmentally friendly and efficient adsorbent for the methylene blue removal from wastewater.

Acknowledgments

We acknowledge the financial support for this work from the Natural Science Foundation of Fujian Province (No. 2019J05127), the Educational Research Project of Young and Middle-aged Teacher of Fujian Province (No. JAT191093), and the Central Government Guides Local Science and Technology Development Project (No. 2019L3013).

References

[1] E. Alver, A.Ü. Metin, F. Brouers, Methylene blue adsorption on magnetic alginate/rice husk bio-composite, Int. J. Biol. Macromol., 154 (2020) 104–113.

[2] B. Ji, L. Zhu, H. Song, W. Chen, S. Guo, F. Chen, Adsorption of methylene blue onto novel biochars prepared from magnolia *Grandiflora linn* fallen leaves at three pyrolysis temperatures, Water Air Soil Pollut., 230 (2019) 281, doi: 10.1007/s11270-019-4330-7.
[3] A. Kundu, A. Mondal, Kinetics, isotherm, and thermodynamic studies of methylene blue selective adsorption and photocatalysis of malachite green from aqueous solution using layered Na-intercalated Cu-doped Titania, Appl. Clay Sci., 183 (2019) 105323, doi: 10.1016/j.clay.2019.105323.
[4] S. Sethi, B.S. Kaith, Saruchi, V. Kumar, Fabrication and characterization of microwave assisted carboxymethyl cellulose-gelatin silver nanoparticles imbibed hydrogel: its evaluation as dye degradation, React. Funct. Polym., 142 (2019) 134–146.
[5] P.K. Malik, S.K. Saha, Oxidation of direct dyes with hydrogen peroxide using ferrous ion as catalyst, Sep. Purif. Technol., 31 (2003) 241–250.
[6] K. Szostak, M. Banach, Sorption and photocatalytic degradation of methylene blue on bentonite-ZnO-CuO nanocomposite, J. Mol. Liq., 286 (2019) 110859, doi: 10.1016/j.molliq.2019.04.136.
[7] D. Ayodhya, G. Veerabhadram, A review on recent advances in photodegradation of dyes using doped and heterojunction based semiconductor metal sulfide nanostructures for environmental protection, Mater. Today Energy, 9 (2018) 83–113.
[8] T.T.V. Tran, S.R. Kumar, S.J. Lue, Separation mechanisms of binary dye mixtures using a PVDF ultrafiltration membrane: Donnan effect and intermolecular interaction, J. Membr. Sci., 575 (2019) 38–49.
[9] K.M. Majewska-Nowak, Application of ceramic membranes for the separation of dye particles, Desalination, 254 (2010) 185–191.
[10] D. Doğan, H. Türkdemir, Electrochemical oxidation of textile dye indigo, J. Chem. Technol. Biotechnol., 80 (2005) 916–923.
[11] L. Gui, J. Peng, P. Li, R. Peng, P. Yu, Y. Luo, Electrochemical degradation of dye on TiO_2 nanotube array constructed anode, Chemosphere, 235 (2019) 1189–1196.
[12] J.M.S. Oliveira, M.R. de Lima e Silva, C.G. Issa, J.J. Corbi, M.H.R.Z. Damianovic, E. Foresti, Intermittent aeration strategy for azo dye biodegradation: a suitable alternative to conventional biological treatments?, J. Hazard. Mater., 385 (2020) 121558, doi: 10.1016/j.jhazmat.2019.121558.
[13] M.M. Martorell, H.F. Pajot, L.I.C.d. Figueroa, Biological degradation of Reactive Black 5 dye by yeast *Trichosporon akiyoshidainum*, J. Environ. Chem. Eng., 5 (2017) 5987–5993.
[14] J. Yang, S. Yu, W. Chen, Y. Chen, Rhodamine B removal from aqueous solution by CT269DR resin: static and dynamic study, Adsorpt. Sci. Technol., 37 (2019) 709–728.
[15] L. Hu, C. Guang, Y. Liu, Z. Su, S. Gong, Y. Yao, Y. Wang, Adsorption behavior of dyes from an aqueous solution onto composite magnetic lignin adsorbent, Chemosphere, 246 (2020) 125757, 10.1016/j.chemosphere.2019.125757.
[16] J.N. Wekoye, W.C. Wanyonyi, P.T. Wangila, M.K. Tonui, Kinetic and equilibrium studies of Congo red dye adsorption on cabbage waste powder, Environ. Chem. Ecotoxicol., 2 (2020) 24–31.
[17] M. Naushad, G. Sharma, Z.A. Alothman, Photodegradation of toxic dye using Gum Arabic-crosslinked-poly(acrylamide)/$Ni(OH)_2$/FeOOH nanocomposites hydrogel, J. Cleaner Prod., 241 (2019) 118263, 10.1016/j.jclepro.2019.118263.
[18] G. Sharma, A. Kumar, M. Naushad, A. Kumar, A.a.H. Al-Muhtaseb, P. Dhiman, A.A. Ghfar, F.J. Stadler, M.R. Khan, Photoremediation of toxic dye from aqueous environment using monometallic and bimetallic quantum dots based nanocomposites, J. Cleaner Prod., 172 (2018) 2919–2930.
[19] S. Chen, Y. Huang, X. Han, Z. Wu, C. Lai, J. Wang, Q. Deng, Z. Zeng, S. Deng, Simultaneous and efficient removal of Cr(VI) and methyl orange on LDHs decorated porous carbons, Chem. Eng. J., 352 (2018) 306–315.
[20] L. Ai, M. Li, L. Li, Adsorption of methylene blue from aqueous solution with activated carbon/cobalt ferrite/alginate composite beads: kinetics, isotherms, and thermodynamics, J. Chem. Eng. Data, 56 (2011) 3475–3483.
[21] N. Somsesta, V. Sricharoenchaikul, D. Aht-Ong, Adsorption removal of methylene blue onto activated carbon/cellulose biocomposite films: equilibrium and kinetic studies, Mater. Chem. Phys., 240 (2020) 122221, doi: 10.1016/j.matchemphys.2019.122221.
[22] B. Huang, R. Zhao, H. Xu, J. Deng, W. Li, J. Wang, H. Yang, L. Zhang, Adsorption of methylene blue on bituminous coal: adsorption mechanism and molecular simulation, ACS Omega, 4 (2019) 14032–14039.
[23] L.C.A. Oliveira, M. Gonçalves, D.Q.L. Oliveira, M.C. Guerreiro, L.R.G. Guilherme, R.M. Dallago, Solid waste from leather industry as adsorbent of organic dyes in aqueous-medium, J. Hazard. Mater., 141 (2007) 344–347.
[24] L. Chen, Y. Li, Q. Du, Z. Wang, Y. Xia, E. Yedinak, J. Lou, L. Ci, High performance agar/graphene oxide composite aerogel for methylene blue removal, Carbohydr. Polym., 155 (2017) 345–353.
[25] A.A. Adeyemo, I.O. Adeoye, O.S. Bello, Adsorption of dyes using different types of clay: a review, Appl. Water Sci., 7 (2017) 543–568.
[26] S. Rahmani, B. Zeynizadeh, S. Karami, Removal of cationic methylene blue dye using magnetic and anionic-cationic modified montmorillonite: kinetic, isotherm and thermodynamic studies, Appl. Clay Sci., 184 (2020) 105391, doi: 10.1016/j.clay.2019.105391.
[27] F. Dhaouadi, L. Sellaoui, G.L. Dotto, A. Bonilla-Petriciolet, A. Erto, A.B. Lamine, Adsorption of methylene blue on comminuted raw avocado seeds: interpretation of the effect of salts via physical monolayer model, J. Mol. Liq., 305 (2020) 112815, doi: 10.1016/j.molliq.2020.112815.
[28] I. Anastopoulos, G.Z. Kyzas, Agricultural peels for dye adsorption: a review of recent literature, J. Mol. Liq., 200 (2014) 381–389.
[29] M. Naushad, A.A. Alqadami, Z.A. AlOthman, I.H. Alsohaimi, M.S. Algamdi, A.M. Aldawsari, Adsorption kinetics, isotherm and reusability studies for the removal of cationic dye from aqueous medium using arginine modified activated carbon, J. Mol. Liq., 293 (2019) 111442, doi: 10.1016/j.molliq.2019.111442.
[30] A.T. Singh, S.K. Ponnuswamy, S.K. K, Synthesis of nano-sized chitosan blended polyvinyl alcohol for the removal of Eosin Yellow dye from aqueous solution, J. Water Process Eng., 13 (2016) 127–136.
[31] T. Tatarchuk, N. Paliychuk, R.B. Bitra, A. Shyichuk, M. Naushad, I. Mironyuk, D. Ziolkovska, Adsorptive removal of toxic Methylene Blue and Acid Orange 7 dyes from aqueous medium using cobalt-zinc ferrite nanoadsorbents, Desal. Water Treat., 150 (2019) 374–385.
[32] G. Bauer, D. Ongari, D. Tiana, P. Gäumann, T. Rohrbach, G. Pareras, M. Tarik, B. Smit, M. Ranocchiari, Metal-organic frameworks as kinetic modulators for branched selectivity in hydroformylation, Nat. Commun., 11 (2020) 1059, doi: 10.1038/s41467-020-14828-6.
[33] D. Barpaga, V.T. Nguyen, B.K. Medasani, S. Chatterjee, B.P. McGrail, R.K. Motkuri, L.X. Dang, Insight into fluorocarbon adsorption in metal-organic frameworks via experiments and molecular simulations, Sci. Rep., 9 (2019) 10289, doi: 10.1038/s41598-019-46269-7.
[34] J. Ren, H.W. Langmi, B.C. North, M. Mathe, D. Bessarabov, Modulated synthesis of zirconium-metal organic framework (Zr-MOF) for hydrogen storage applications, Int. J. Hydrogen Energy, 39 (2014) 890–895.
[35] J. Cavka, S. Jakobsen, U. Olsbye, N. Guillou, C. Lamberti, S. Bordiga, K. Lillerud, A new zirconium inorganic building brick forming metal organic frameworks with exceptional stability, J. Am. Chem. Soc., 130 (2008) 13850–13851.
[36] P. Yang, Q. Liu, J. Liu, H. Zhang, Z. Li, R. Li, L. Liu, J. Wang, Interfacial growth of metal organic framework (UiO-66) on the functionalization of graphene oxide (GO) as a suitable seawater adsorbent for extraction of uranium(VI), J. Mater. Chem. A, 5 (2017) 17933–17942.
[37] I. Ahmed, N.A. Khan, S.H. Jhung, Adsorptive denitrogenation of model fuel by functionalized UiO-66 with acidic and basic moieties, Chem. Eng. J., 321 (2017) 40–47.

[38] P.W. Seo, I. Ahmed, S.H. Jhung, Adsorptive removal of nitrogen-containing compounds from a model fuel using a metal–organic framework having a free carboxylic acid group, Chem. Eng. J., 299 (2016) 236–243.
[39] L. Abramian, H. El-Rassy, Adsorption kinetics and thermodynamics of azo-dye Orange II onto highly porous titania aerogel, Chem. Eng. J., 150 (2009) 403–410.
[40] M.E. Argun, S. Dursun, C. Ozdemir, M. Karatas, Heavy metal adsorption by modified oak sawdust: thermodynamics and kinetics, J. Hazard. Mater., 141 (2007) 77–85.
[41] A.S. Eltaweil, G.S. Elgarhy, G.M. El-Subruiti, A.M. Omer, Carboxymethyl cellulose/carboxylated graphene oxide composite microbeads for efficient adsorption of cationic methylene blue dye, Int. J. Biol. Macromol., 154 (2020) 307–318.
[42] M. Ghaedi, A. Hassanzadeh, S. Kokhdan, Multiwalled carbon nanotubes as adsorbents for the kinetic and equilibrium study of the removal of alizarin red s and morin, J. Chem. Eng. Data, 56 (2011) 2511–2520.
[43] Y.S. Ho, Selection of optimum sorption isotherm, Carbon, 42 (2004) 2115–2116.
[44] N.T. Hai, S.J. You, H.P. Chao, Thermodynamic parameters of cadmium adsorption onto orange peel calculated from various methods: a comparison study, J. Environ. Chem. Eng., 4 (2016) 2671–2682.
[45] O. Pezoti, A.L. Cazetta, K.C. Bedin, L.S. Souza, A.C. Martins, T.L. Silva, O.O. Santos Júnior, J.V. Visentainer, V.C. Almeida, NaOH-activated carbon of high surface area produced from guava seeds as a high-efficiency adsorbent for amoxicillin removal: kinetic, isotherm and thermodynamic studies, Chem. Eng. J., 288 (2016) 778–788.
[46] S. Norouzi, M. Heidari, V. Alipour, O. Rahmanian, M. Fazlzadeh, F. Mohammadi-moghadam, H. Nourmoradi, B. Goudarzi, K. Dindarloo, Preparation, characterization and Cr(VI) adsorption evaluation of NaOH-activated carbon produced from Date Press Cake; an agro-industrial waste, Bioresour. Technol., 258 (2018) 48–56.
[47] P.S. Ghosal, A.K. Gupta, Determination of thermodynamic parameters from Langmuir isotherm constant-revisited, J. Mol. Liq., 225 (2017) 137–146.
[48] F. An, R. Wu, M. Li, T. Hu, J. Gao, Z. Yuan, Adsorption of heavy metal ions by iminodiacetic acid functionalized D301 resin: kinetics, isotherms and thermodynamics, React. Funct. Polym., 118 (2017) 42–50.
[49] E.C. Lima, A. Hosseini-Bandegharaei, J.C. Moreno-Piraján, I. Anastopoulos, A critical review of the estimation of the thermodynamic parameters on adsorption equilibria, wrong use of equilibrium constant in the Van't Hoof equation for calculation of thermodynamic parameters of adsorption, J. Mol. Liq., 273 (2019) 425–434.
[50] I. Anastopoulos, G.Z. Kyzas, Are the thermodynamic parameters correctly estimated in liquid-phase adsorption phenomena?, J. Mol. Liq., 218 (2016) 174–185.
[51] Uma, S. Banerjee, Y.C. Sharma, Equilibrium and kinetic studies for removal of malachite green from aqueous solution by a low cost activated carbon, J. Ind. Eng. Chem., 19 (2013) 1099–1105.
[52] M.J. Ahmed, Application of agricultural based activated carbons by microwave and conventional activations for basic dye adsorption: review, J. Environ. Chem. Eng., 4 (2016) 89–99.
[53] F. Wu, R. Tseng, R. Juang, Characteristics of Elovich equation used for the analysis of adsorption kinetics in dye-chitosan systems, Chem. Eng. J., 150 (2009) 366–373.
[54] A.C. Martins, O. Pezoti, A.L. Cazetta, K.C. Bedin, D.A.S. Yamazaki, G.F.G. Bandoch, T. Asefa, J.V. Visentainer, V.C. Almeida, Removal of tetracycline by NaOH-activated carbon produced from macadamia nut shells: kinetic and equilibrium studies, Chem. Eng. J., 260 (2015) 291–299.
[55] C.H. Weng, Y.T. Lin, T.W. Tzeng, Removal of methylene blue from aqueous solution by adsorption onto pineapple leaf powder, J. Hazard. Mater., 170 (2009) 417–424.
[56] W.H. Cheung, Y.S. Szeto, G. McKay, Intraparticle diffusion processes during acid dye adsorption onto chitosan, Bioresour. Technol., 98 (2007) 2897–2904.
[57] G.L. Dotto, L.A.A. Pinto, Adsorption of food dyes acid blue 9 and food yellow 3 onto chitosan: stirring rate effect in kinetics and mechanism, J. Hazard. Mater., 187 (2011) 164–170.
[58] Q.X. Liu, Y.R. Zhou, M. Wang, Q. Zhang, T. Ji, T.Y. Chen, D.C. Yu, Adsorption of methylene blue from aqueous solution onto viscose-based activated carbon fiber felts: kinetics and equilibrium studies, Adsorpt. Sci. Technol., 37 (2019) 312–332.
[59] D.K. Mahmoud, M.A.M. Salleh, W.A.W.A. Karim, A. Idris, Z.Z. Abidin, Batch adsorption of basic dye using acid treated kenaf fibre char: equilibrium, kinetic and thermodynamic studies, Chem. Eng. J., 181–182 (2012) 449–457.
[60] C.A. Başar, Applicability of the various adsorption models of three dyes adsorption onto activated carbon prepared waste apricot, J. Hazard. Mater., 135 (2006) 232–241.
[61] S. Banerjee, R.K. Gautam, A. Jaiswal, M. Chandra Chattopadhyaya, Y. Chandra Sharma, Rapid scavenging of methylene blue dye from a liquid phase by adsorption on alumina nanoparticles, RSC Adv., 5 (2015) 14425–14440.
[62] A. Aygün, S. Yenisoy-Karakaş, I. Duman, Production of granular activated carbon from fruit stones and nutshells and evaluation of their physical, chemical and adsorption properties, Microporous Mesoporous Mater., 66 (2003) 189–195.
[63] S.H. Siddiqui, The removal of Cu_2^+, Ni_2^+ and Methylene Blue (MB) from aqueous solution using *Luffa actangula* carbon: kinetics, thermodynamic and isotherm and response methodology, Groundwater Sustainable Dev., 6 (2018) 141–149.